IEEE Access
Multidisciplinary | Rapid Review | Open Access Journal

Received May 8, 2021, accepted May 24, 2021, date of publication May 27, 2021, date of current version June 7, 2021.

Digital Object Identifier 10.1109/ACCESS.2021.3084403

Design Evolution of the Ultrasonic Piezoelectric Motor Using Three Rotating Mode Actuators

ROLAND RYNDZIONEK[1], (Member, IEEE), ŁUKASZ SIENKIEWICZ[1], MICHAŁ MICHNA[1], (Senior Member, IEEE), AND MAREK CHODNICKI[2]

[1]Faculty of Electrical and Control Engineering, Gdańsk University of Technology, 80-233 Gdańsk, Poland
[2]Faculty of Mechanical Engineering and Ship Technology, Gdańsk University of Technology, 80-233 Gdańsk, Poland

Corresponding author: Roland Ryndzionek (roland.ryndzionek@pg.edu.pl)

ABSTRACT The development process and experimental investigation of the multicell piezoelectric motor is presented in this paper. The proposed design consists of three individual cells integrated into the stator, double rotor, and a preload system. Those elements are combined into a symmetrical structure of the motor. The two new prototypes have been designed, simulated and tested. Finite element numerical analysis is carried out to obtain optimal dimensions of the individual cell in terms of generated vibrations and resonant frequencies of the structure. The results of the numerical analysis are compared with analytical calculations based on the equivalent circuit model. The stator of the motor was manufactured using a three-dimensional (3-D) printer using alumide material. Finally, the experimental tests were conducted and presented. Analytical, numerical and experimental results are in satisfactory agreement. Two new prototypes of the multicell piezoelectric motor exhibit torque-speed characteristics similar to the original while being cheaper and easier to manufacture.

INDEX TERMS Piezoelectric actuator, piezoelectric ultrasonic motor, piezoelectricity, travelling wave motor, rotary motor.

I. INTRODUCTION

Through the last decade, piezoelectric technology has experienced steady growth [1]–[6]. At present, transducers that utilize the converse piezoelectric effect, available on the market, are divided into two major types: ultrasonic and quasi-static [7]–[10]. Moreover, the ultrasonic motors (USM) are classified into travelling wave ultrasonic motors (TWUM) and standing wave ultrasonic motors (SWUM). Another accepted classification of piezoelectric motors takes into account the characteristics of the output motion in terms of degrees of freedom (DOF). Rotary and linear designs belong to a single DOF sub-category. Spherical, planar, and rotary-linear motors exhibit a rotation around 2 or 3 axes, linear motion along two axes or a combination of rotation and linear movement along one axis. Such multi-DOF motors have the advantage in applications requiring high functionality in limited package [11]–[14]. Moreover, the multi-DOF motors need a dedicated and often complex power system supply, requiring a multi-level power supply in general [15]–[18].

The associate editor coordinating the review of this manuscript and approving it for publication was Yingxiang Liu.

Among the existing piezoelectric materials, hard PZT ceramics have the highest applicability in the field of electromechanical transducers. Moreover, ongoing developments in material engineering result in optimization of the desirable properties of active materials. Such physical properties as low dielectric losses and favourable piezoelectric constants in a wide temperature range are crucial in the ultrasonic motor's development [19], [20].

Modern USMs generally exhibit high torque density in comparison to traditional electric motors. Thus, USMs are well suited for applications requiring high degree miniaturization combined with high speed and load abilities [21]. Some authors report on USMs used in extreme environments such as: the minor planet and deep sea exploration [22], [23]. In general, TWUM is the most widely known representative of ultrasonic motors [24], [25]. The principle of operation is based on the making of a travelling wave on the surface of the stator. The TWUM utilizes the elliptical motions, which are generated by the converse piezoelectric effects of the piezoelectric elements, and friction coupling between the rotor and the stator to drive the rotor [26]–[28].

This paper is the result of further research and development under the Multicell Piezoelectric Motor (MPM) [29].

The main objective is a comparison between existing MPM and newly developed prototypes in terms of mechanical characteristics. The structure of the developed motors is introduced, and its principle of operation is described in section II. The FEM simulation of new MPMs in ANSYS environment is presented in section III. In section IV, manufacturing of the prototypes and experimental analysis are explained. Finally, the paper ends with a summary of the obtained results.

II. PROJECT DESCRIPTION

The original objective of the research on MPM was to develop a structure which will combine the topology of the travelling wave and rotating-mode motors and will operate in the ultrasonic range. The main goal behind the development of the latest prototypes was a simplification of the mechanical structure while maintaining the favourable torque-speed characteristics of the first iteration. The authors used rapid prototyping techniques, such as metal 3-D printing during the manufacturing process. Such an approach helped with faster and cheaper prototype preparation than more traditional manufacturing techniques, such as CNC machining from steel or aluminium. The MPM was introduced for the first time in a conference paper [30] where the principle and basic laboratory tests have been presented. In parallel, the analytical study has been carried out and described in [31]. The work on first MPM revision (MPM basic) has been summarized in [29] and an extended version (with updated prototype) has been reported in [32]. In this paper, the authors describe the evolution of the design and analyse the newly developed MPM prototypes (MPM No. 1 and No. 2) in terms of torque-speed characteristics.

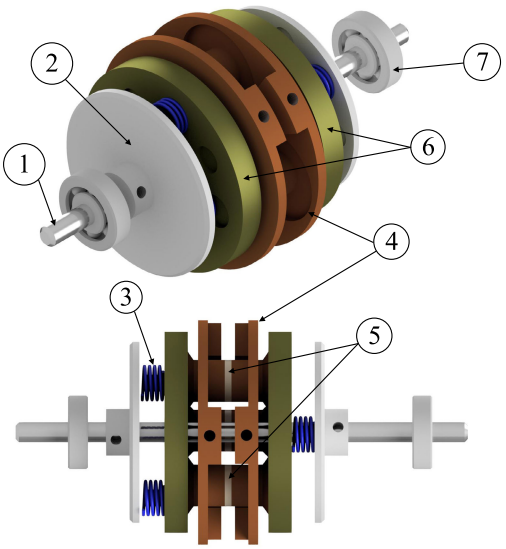

FIGURE 1. The structure of MPM basic prototype where: 1 shaft, 2 ending plate, 3 spring, 4 stator with three actuators, 5 piezoelectric ceramics, 6 rotor and 7 bearing.

Multicell piezoelectric motor (Figure 1) employs three actuators in its structure, which can be considered as independent cells. Such an approach enables symmetry and supports

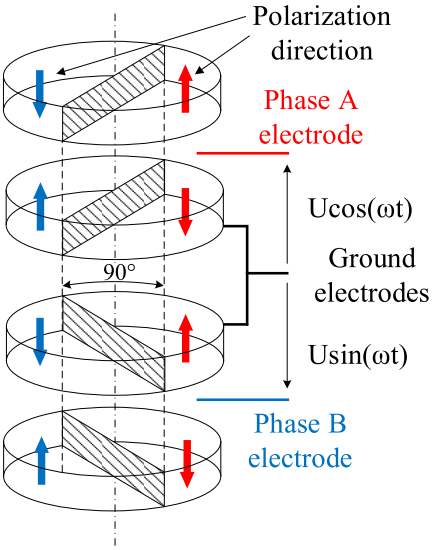

FIGURE 2. The piezoelectric ceramics orientation of MPM prototype in single actuator.

a more stable assembly than a single actuator design. Each of MPM's cells resembles the build of a Langevin transducer, with two pairs of piezoelectric ceramics inserted between two counter-masses. In contrast to the Langevin design, a single MPM cell generates two bending modes. This is achieved by two sets of sectorized piezoelectric ceramics, orthogonally placed to each other. An elliptic motion is created on the surface of each cell by a superposition of the bending modes when the ceramics are supplied with two sinusoidal, high-frequency voltage sources with a 90° phase shift (Figure 2). A sandwich of two ceramic pairs and metal counter-masses is used to amplify the vibrations generated by the ceramics. Three cells of the MPM will generate three travelling waves driving the rotors.

Compared to the MPM basic prototype (Figure 1), the new structure has been modified in some aspects. In previous versions multiple technical issues with the correct rotor-stator adjustment have been identified. The authors have decided to simplify the single actuator shape compared to the original geometry (Figure 3) [30]. The diameter and length of the stator is equal to 67 and 16 mm, respectively. Each of the three actuators has a diameter of 12.5 mm, which also equals the external diameter of the ceramics. The PZTs used in the actuators have an internal diameter of 5 mm and thickness of 0.5 mm. The contact surface between the rotor and the stator has been modified compared to the previous prototypes [31]. The MPM No. 1 (Figure 3a) has flat surface while the MPM No. 2 (Figure 3b) has small teeth on a third of the circumference to modify the contact conditions.

The manufacturing time and cost were important aspects in the development of motor prototypes. The stator was manufactured using additive manufacturing (3D printing) with Direct Metal Laser Sintering/Selective Laser Sintering (DMLS/SLS) technology. To further reduce the price, the authors decided to use the alumide material (polyamide filled with aluminum dust) for stator, as this material is

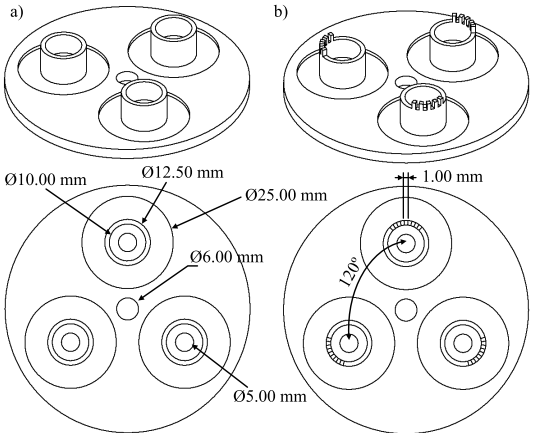

FIGURE 3. The structure of the stator in configuration: a) No.1 and b) No.2.

TABLE 1. Main material properties of Alumide and NCE81 ceramics used in the MPM stator.

Parameter	Symbol	Model value
NCE81 Relative dielectric constant [-]	$\varepsilon_{33}^{T}/\varepsilon_0$	1020
NCE81 Coupling factors [-]	k_{31} k_{33} k_{31}	0.30 0.69 0.47
NCE81 Charge constant [10^{-12} C/N]	d_{31} d_{33}	-108 -269
NCE81 Quality factor [-]	Q_M	1400
NCE81 Density [kg/m^3]	ρ_{PZT}	7730
Alumide Young's modulus [10^9 Pa]	E	3.6
Alumide Density [kg/m^3]	ρ_A	1300
Alumide Poisson's ratio [-]	ν	0.35

cheaper than regular aluminium (and much cheaper than aluminum stator made with CNC technology). The mechanical properties of alumide can vary depending on the orientation of the samples manufactured by DMLS/SLS technology [33]. The following values were used in analytical and FEM analysis: a mass density of 1300 kg/m^3, a Young's modulus of 3.6 $\times$ 10^9 Pa, and a Poisson ratio of 0.35. The material of the ceramic ring was NCE81 PZT (provided by Noliac). Main material properties of the stator are presented in Table 1. The rotor has been manufactured in three variants made from steel, aluminum and polylactic acid (PLA).

The cross-section of the full structure is presented in Figure 4 (No. 1 configuration). Due to its geometrical design, use of two rotors is possible and favourable for increasing the mechanical output of the motor. Furthermore, to improve the contact conditions, the rotor can be adjusted to the stator with help of Smalley type springs (model CMS14-L4).

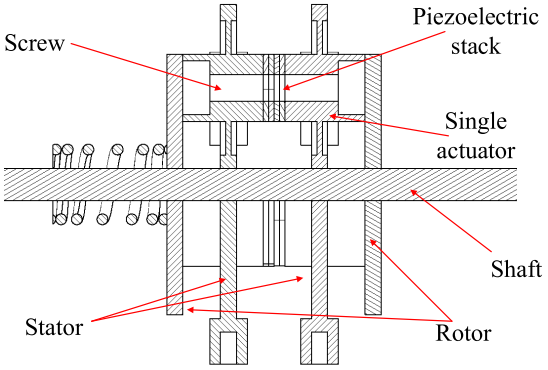

FIGURE 4. Cross-section of the full MPM structure with stator in No. 1 configuration.

III. FEA SIMULATION

Finite element analysis (FEA) is the most common method in designing piezoelectric actuators or other electromechanical systems or structures. In the case of Ultrasonic motors, FEA is often used to examine the natural frequencies of the investigated structure as a function of its geometry and assigned material properties. The authors performed a modal analysis to obtain the resonance frequency of actuators in the ultrasonic range. Several modes were observed in a 20 kHz–100 kHz frequency range. The calculations for MPM No.1 and No. 2 were carried out using ANSYS Workbench software and used to select the appropriate structure for a single actuator. The mesh was generated using adaptive refinement controlled by software. The final mesh included 23k nodes and 13k elements. Such mesh density allowed achieving satisfactory results in a reasonable amount of time. The stator has been fixed on the bottom side, on the internal and the external sidewall to satisfy the boundary conditions (Figure 5). The stator's material for the analysis was Alumide.

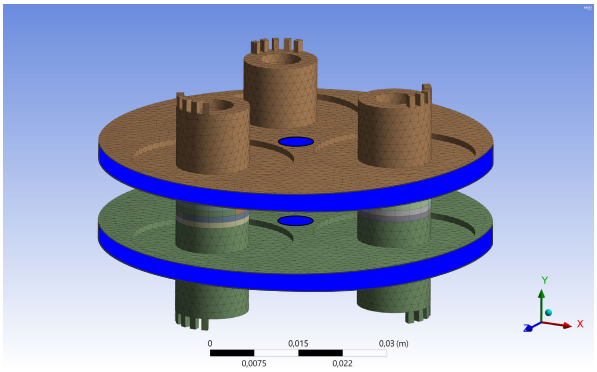

FIGURE 5. Boundary conditions for modal analysis of MPM. Blue areas indicate fixed surfaces.

The modal analysis returned several resonance frequencies. However, the authors considered only the two bending modes necessary for the creation of the travelling wave. The other frequencies linked with respiration modes or with parasitic deformations of the armature were not considered in

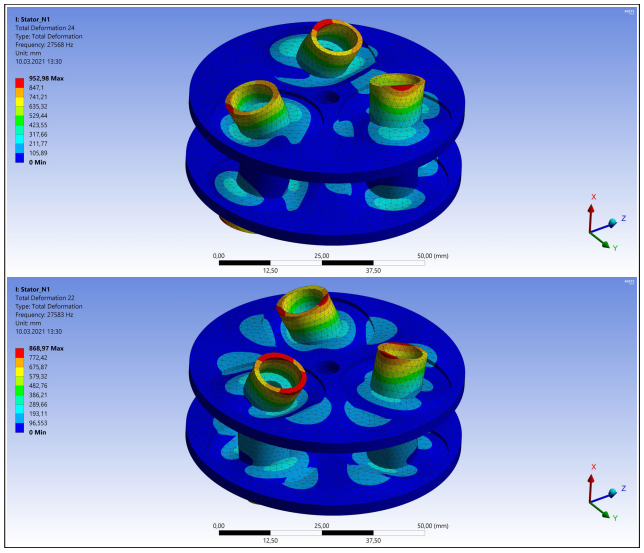

FIGURE 6. The results of modal analysis of MPM No. 1: the first bending vibration mode and the second bending vibration mode.

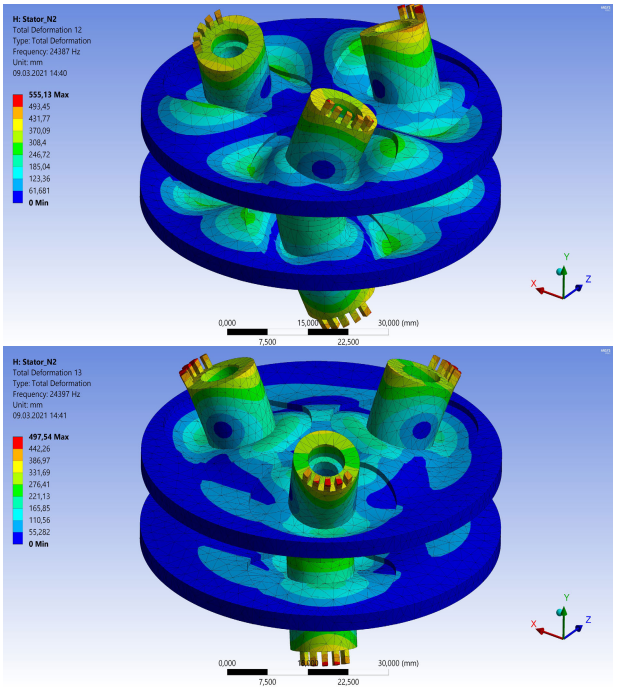

FIGURE 7. The results of modal analysis of MPM No. 2: the first bending vibration mode and the second bending vibration mode.

MPM development and as a consequence, are not presented below. As shown in Figure 6, the first bending mode and the second bending mode of MPM No. 1 are 27 568 kHz, 27 583 kHz, respectively.

In Figure 7, the first bending mode and the second bending mode of MPM No. 2 are 24 387 kHz, 24 397 kHz, respectively. All results are in the ultrasonic range so the main goal of MPM's development has been achieved.

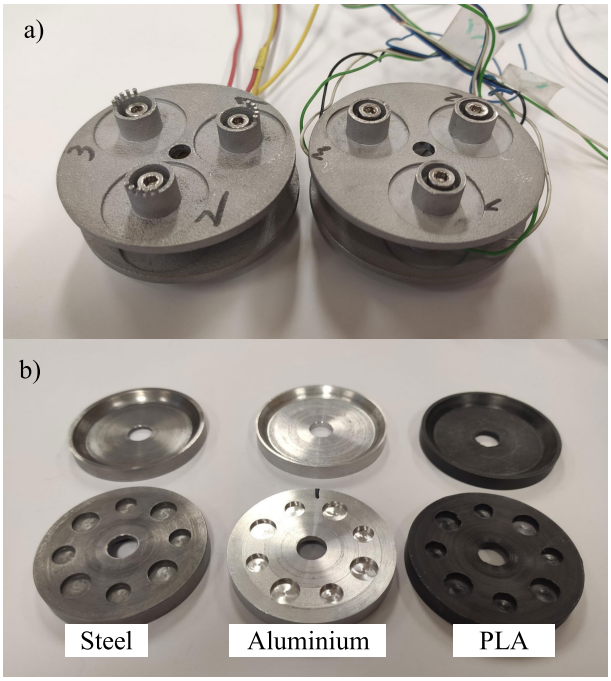

FIGURE 8. Manufactured MPM No. 1 and No. 2: (a) Stator in two configurations. (b) Rotors made from three materials.

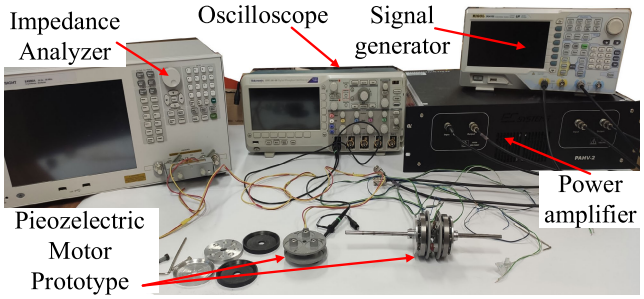

FIGURE 9. The test bench for experimental setup of proposed MPM structures.

IV. EXPERIMENTAL RESULTS

Two new prototypes of MPM (No. 1 and No. 2) have been manufactured and assembled. The stator is shown in Figure 8a. As was mentioned in the previous section, the stator was 3D printed from Alumide. Due to the used technology, the prototypes are not as precisely manufactured, as with CNC technology. The surfaces are slightly rough and more susceptible to failure compared to a solid aluminium block. The rotor was manufactured in three variants using steel, aluminium and PLA materials (Figure 8b). The test bench has been presented in Figure 9.

The experimental analysis began with resonance frequency measurements for all three actuators by the Keysight E4990A Impedance Analyzer. An essential aspect of this stage was to obtain similar resonance frequencies for all three actuators. The resonance frequency depended heavily on the

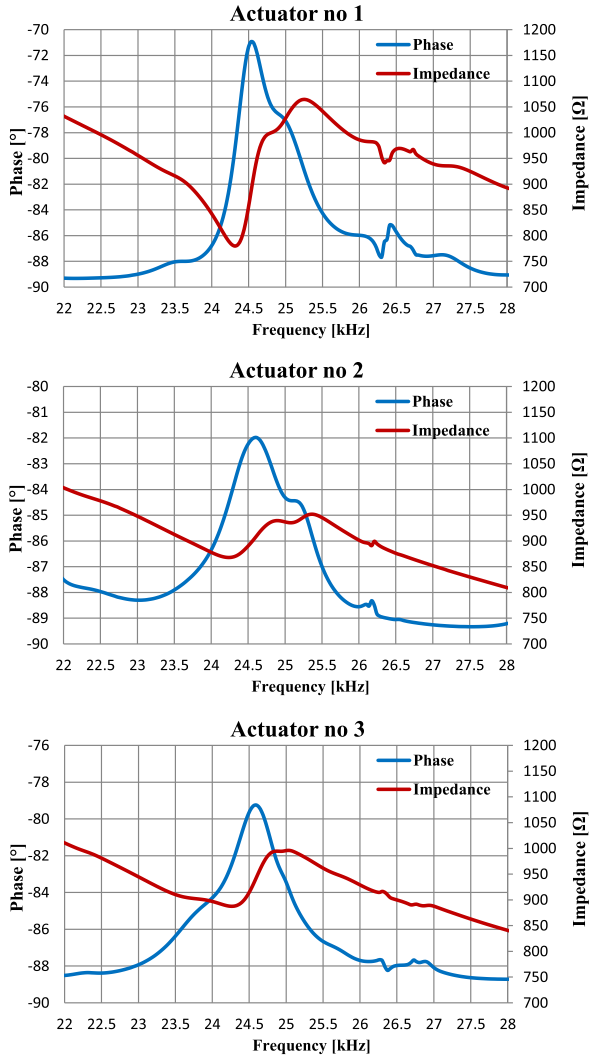

FIGURE 10. Results of the resonance frequency measurements for each actuator in prototype MPM No. 1, where the red line is impedance and the blue line is phase.

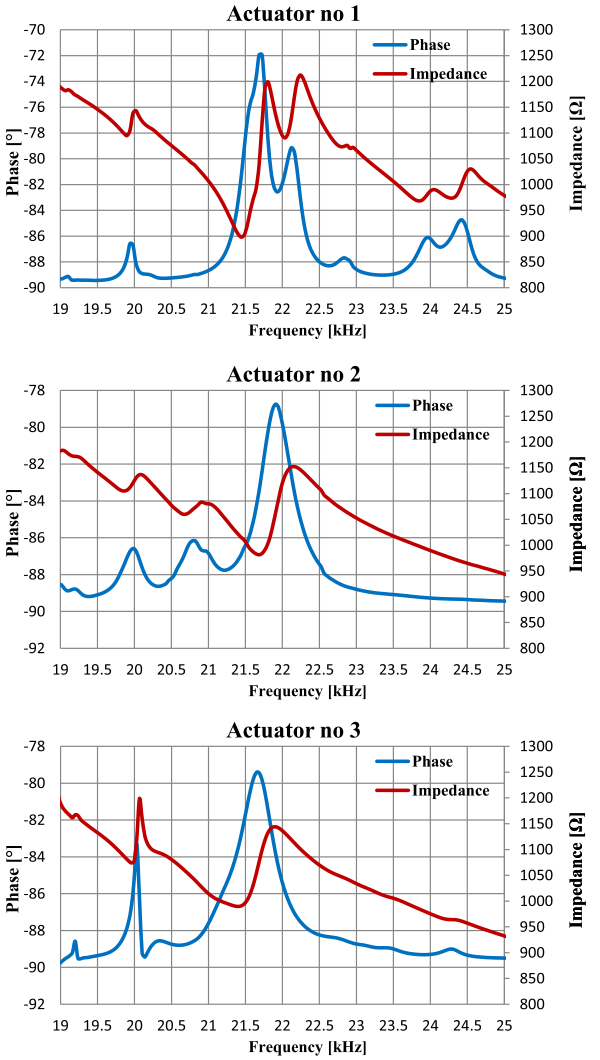

FIGURE 11. Results of the resonance frequency measurements for each actuator in prototype MPM No. 2, where the red line is impedance and the blue line is phase.

force applied by the screw as well as the tightening torque. In MPM No. 1, the measured resonance frequency was between 24.25-24.40 kHz for all three actuators. Furthermore, in MPM No. 2, the measured resonance frequency was between 21.5-21.6 kHz for all three actuators. Frequency and phase plots have been presented in Figure 10 and Figure 11 for MPM No. 1 and MPM No. 2, respectively.

The differences between measured and simulated resonance frequencies for MPM No. 1 and No. 2 are approximately 4 and 4.5 kHz, respectively. Furthermore, the difference in measured frequency values between MPM No.1 and MPM No.2 is roughly 2.7 kHz. As has been stated in the previous paragraph, the resonance point depends, among other factors, on the force applied by the screw. On one hand, the authors decided not to use a higher tightening force, due to the risk of damaging the stator. On the other hand, simulated resonance frequencies for MPM No.1 and MPM No. 2 have about 2.2 kHz difference. Thus, simulation results correspond to the measured results, following similar frequency difference between the prototypes and are in a satisfactory range above 20 kHz. In general, the agreement between FEA and measurement results is far more than acceptable.

Finally, the electromechanical characteristics of both prototypes were measured. To obtain the optimum MPM operation conditions, two alternating voltages with 90° phase difference and the amplitude of 200 Vp-p were applied to the corresponding electrodes. A high-voltage linear amplifier PAHV-2 was controlled by a Rigol DG4102 signal generator to set the voltage frequency as close to the frequency of mechanical resonance (Figure 9).

The influence of the frequency change on the rotary speed was measured by a digital, non-contact laser velocimeter. As expected, the highest speed of MPM No. 1 has been

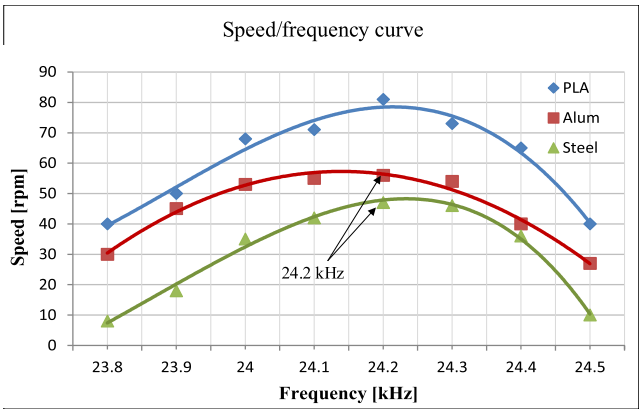

FIGURE 12. Experimental analysis of MPM No. 1: speed versus excitation frequency for rotors made from PLA (blue trace), Aluminum (red trace) and Steel (green trace).

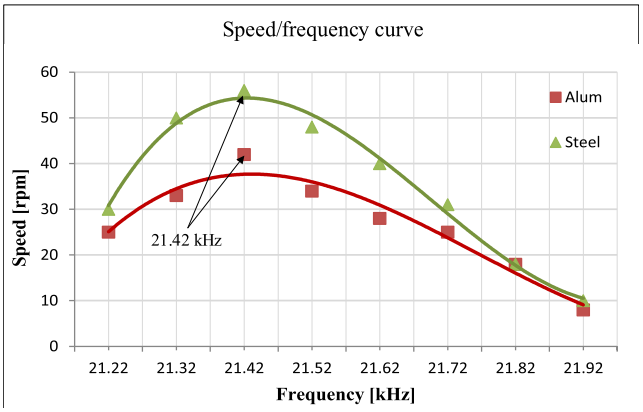

FIGURE 13. Experimental analysis of MPM No. 2: speed versus excitation frequency for rotors made from Aluminum (red trace) and Steel (green trace).

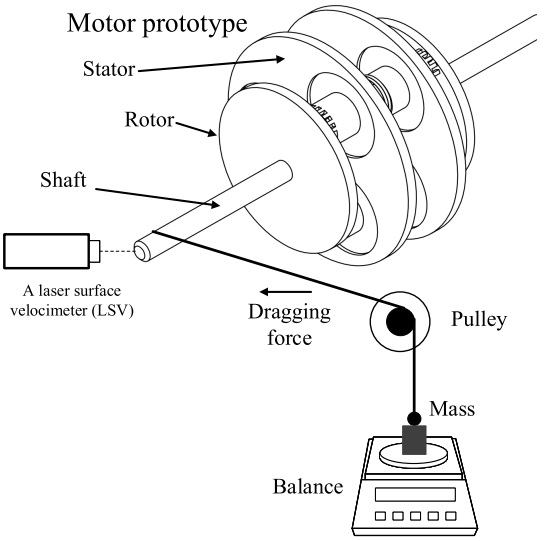

FIGURE 14. The test bench for stall torque measurements.

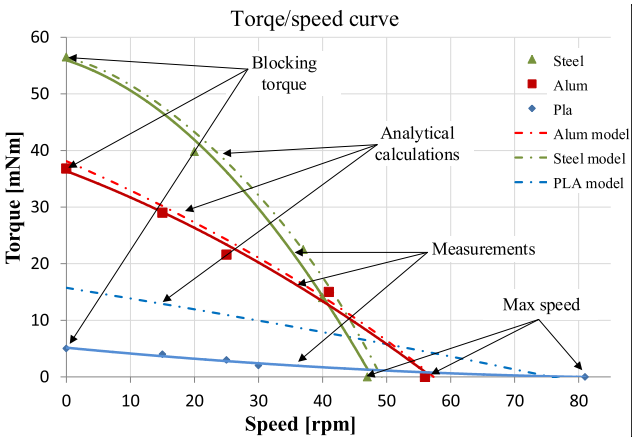

FIGURE 15. Experimental analysis of MPM No. 1: torque versus speed for rotors made from PLA (blue trace), Aluminum (red trace) and Steel (green trace). Comparison of measured and calculated torque-speed characteristics of MPM No. 1. with rotors made of different materials. Points and solid lines correspond to measurements, while the dashed lines correspond to analytical calculations.

achieved with a PLA rotor. However, it was not possible to measure the speed for PLA rotor in combination with MPM No. 2 as the 3-D printed rotor movement was intermittent. In both cases, the speed-frequency characteristics for steel and aluminium rotors showcased similar performance (Figure 12 and Figure 13). The highest values have been achieved in the same resonance frequency of 24.2 kHz and 21.42 kHz for MPM No. 1 and No. 2, respectively.

The setup for the stall torque measurement is presented in Figure 14. A weight was linked to the motor's shaft by a copper wire. An electronic balance was used to specify the mass. During the motor operation, the output torque was transferred into a dragging force upon the weight. The torque has been calculated by multiplying the dragging force and the radius of the rotor.

The following stage of experimental analysis was measurement of torque-speed characteristics (Figure 15 and Figure 16). With the power supply limitations listed in the previous paragraphs, the measured blocking torque (steel rotor) was 0.057 Nm and 0.068 Nm for MPM No. 1 and No. 2.

Based on calculations described in [29], [31], [32] a torque versus speed analytical characteristic has been determined. The MPM geometrical parameters mentioned in chapter 2 were used. The comparison of analytical and experimental characteristics (Figure 15) results in good agreement for MPM prototype No. 1 with rotor made of steel and aluminum but a greater difference, especially in terms of maximal torque value, for rotor 3D printed from PLA. This may be caused by a discrepancy in terms of mechanical properties between raw material and printed rotor.

Finally, the influence of the voltage change on the rotary speed was measured (Figure 17). As expected, the rotary speed changes linearly in relation to the voltage. Due to the power supply limitations the maximal voltage was 200 Vp-p.

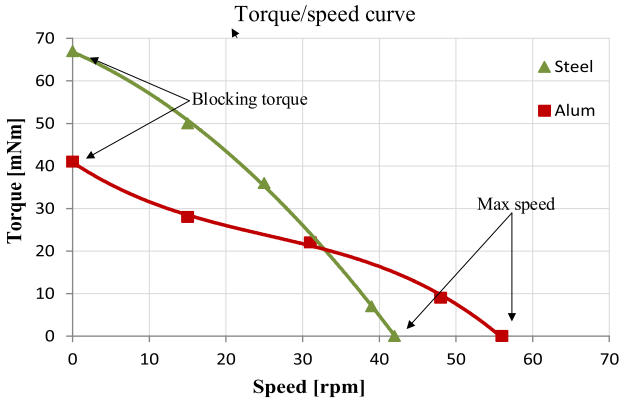

FIGURE 16. Experimental analysis of MPM No. 2: torque versus speed for rotors made from Aluminum (red trace) and Steel (green trace).

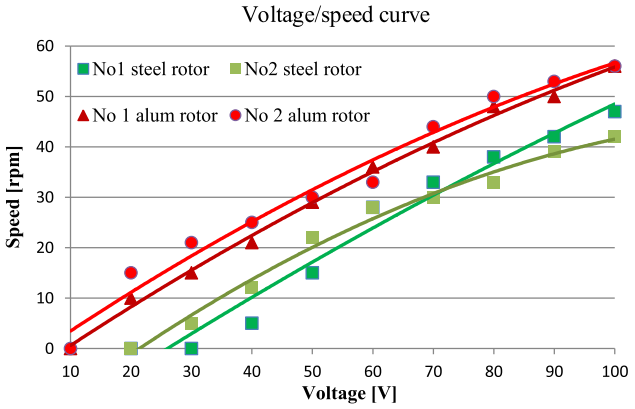

FIGURE 17. Experimental analysis: rotary speed versus voltage for MPM No. 1 and No. 2 with rotors made of Steel (red traces) and Aluminum (green traces).

Higher rotary speed and torque can be achieved by increasing the output voltage of the power amplification stage.

V. CONCLUSION

In this paper, improved prototypes of an ultrasonic piezoelectric motor using three rotating mode actuators referred to as a ''multicell piezoelectric motor'' were developed and tested. Moreover, the motors have been tested with different rotor materials. The new prototype (MPM No. 2) has a 13% higher maximum torque compared to the MPM basic prototype. However, the main advantage was a simplification of the mechanical structure and manufacturing of the prototypes using faster and cheaper technology. The cost of prototype fabrication was 41% lower for the 3D printing from Alumide compared to the traditional CNC technique.

The FEA analysis has been computed in ANSYS software to determine the resonance frequencies of two prototypes. The frequency values were around 27.57 kHz and 24.4 kHz for MPM No. 1 and No. 2 respectively. Finally, both prototypes have been manufactured and tested in the laboratory. It should be noted that stator material (Alumide) of MPM No. 1 and No. 2 has approximately two times smaller density and Young's modulus than the basic MPM version.

TABLE 2. The performance of MPM prototypes (steel rotor).

Parameter	MPM basic [32]	MPM No. 1	MPM No. 2
Driving signal [V_{p-p}]	200	200	200
Resonance freq. [kHz] measurements	24.63	24.2	21.42
Resonance freq. [kHz] simulations	25.6	27.57	24.4
Max speed [rpm]	63	48	42
Blocking torque [Nm]	0.06	0.057	0.068
Active Volume [m^3]	2.06e-7	2.06e-7	2.06e-7
Motor's Size [mm]	38x67	42x67	46x67
Motor's Weight [g]	350	328	330

However, the mechanical parameters of the new prototypes like speed and torque show good performance. The maximum blocking torque achieved in MPM No. 2 is the highest registered value. Thus, it can be assumed that a structure using aluminum stator will have even better performance. This will be investigated in future research. The significant parameters of all MPM prototypes have been compared and presented in Table 2.

Based on this research, the authors are developing a new structure which will have better performance. It is planned to use three driving rotors and one shaft.

REFERENCES

[1] K. Uchino, "Piezoelectric actuator renaissance," *Energy Harvesting Syst.*, vol. 1, nos. 1–2, pp. 45–56, Jan. 2014. [Online]. Available: www.murata.co.jp/corporate/ad/article/metamorpho-
[2] L. Wang, W. Chen, J. Liu, J. Deng, and Y. Liu, "A review of recent studies on non-resonant piezoelectric actuators," *Mech. Syst. Signal Process.*, vol. 133, Nov. 2019, Art. no. 106254. [Online]. Available: https://linkinghub.elsevier.com/retrieve/pii/S0888327019304698
[3] W. Xu and Y. Wu, "Piezoelectric actuator for machining on macro-to-micro cylindrical components by a precision rotary motion control," *Mech. Syst. Signal Process.*, vol. 114, pp. 439–447, Jan. 2019.
[4] J. Niu, J. Wu, M. Cao, and L. Wu, "A traveling-wave linear ultrasonic motor driven by two torsional vibrations: Design, fabrication, and performance evaluation," *IEEE Access*, vol. 8, pp. 122554–122564, 2020. [Online]. Available: https://ieeexplore.ieee.org/document/9133076/
[5] X. Li, C. Kan, Y. Cheng, Z. Chen, and T. Ren, "Performance evaluation of a bimodal standing-wave ultrasonic motor considering nonlinear electroelasticity: Modeling and experimental validation," *Mech. Syst. Signal Process.*, vol. 141, Jul. 2020, Art. no. 106475.
[6] L. Wang, Y. Liu, Q. Shen, and J. Liu, "Design and experimental verification of a bolt-clamped piezoelectric actuator based on clamping and driving mechanism," *Mech. Syst. Signal Process.*, vol. 146, Jan. 2021, Art. no. 107065.
[7] S.-T. Ho and S.-J. Jan, "A piezoelectric motor for precision positioning applications," *Precis. Eng.*, vol. 43, pp. 285–293, Jan. 2016.
[8] Y. Liu, J. Deng, and Q. Su, "Review on multi-degree-of-freedom piezoelectric motion stage," *IEEE Access*, vol. 6, pp. 59986–60004, 2018.
[9] Y. Liu, W. Chen, J. Liu, and S. Shi, "A high-power linear ultrasonic motor using longitudinal vibration transducers with single foot," *IEEE Trans. Ultrason., Ferroelectr., Freq. Control*, vol. 57, no. 8, pp. 1860–1867, Aug. 2010.
[10] Y. Wang, Q. Quan, H. Yu, D. Bai, H. Li, and Z. Deng, "Rotary-percussive ultrasonic drill: An effective subsurface penetrating tool for minor planet exploration," *IEEE Access*, vol. 6, pp. 37796–37806, 2018.

[11] S. Wang, W. Rong, L. Wang, H. Xie, L. Sun, and J. K. Mills, "A survey of piezoelectric actuators with long working stroke in recent years: Classifications, principles, connections and distinctions," *Mech. Syst. Signal Process.*, vol. 123, pp. 591–605, May 2019.
[12] V. Jūrėnas, G. Kazokaitis, and D. Mažeika, "3DOF ultrasonic motor with two piezoelectric rings," *Sensors*, vol. 20, no. 3, p. 834, Feb. 2020. [Online]. Available: https://www.mdpi.com/1424-8220/20/3/834
[13] N. Chen, J. Zheng, and D. Fan, "Pre-pressure optimization for ultrasonic motors based on multi-sensor fusion," *Sensors*, vol. 20, no. 7, p. 2096, Apr. 2020. [Online]. Available: https://www.mdpi.com/1424-8220/20/7/2096
[14] H. Yu, Q. Quan, X. Tian, and H. Li, "Optimization and analysis of a U-shaped linear piezoelectric ultrasonic motor using longitudinal transducers," *Sensors*, vol. 18, no. 3, p. 809, Mar. 2018. [Online]. Available: http://www.mdpi.com/1424-8220/18/3/809
[15] R. Li, N. Frohleke, and J. Bocker, "LLCC-PWM inverter for driving high-power piezoelectric actuators," in *Proc. 13th Int. Power Electron. Motion Control Conf.*, Sep. 2008, pp. 159–164.
[16] C. I. Odeh, A. Lewicki, and M. Morawiec, "A single-carrier-based pulse-width modulation template for cascaded H-bridge multilevel inverters," *IEEE Access*, vol. 9, pp. 42182–42191, 2021.
[17] D. Makowski, A. Mielczarek, P. Perek, A. Szubert, P. Plewinski, G. Jablonski, W. Cichalewski, and A. Napieralski, "High-power piezoelectric tuner driver for lorentz force compensation," *IEEE Trans. Nucl. Sci.*, vol. 66, no. 7, pp. 1056–1063, Jul. 2019.
[18] C. I. Odeh, A. Lewicki, M. Morawiec, and D. Kondratenko, "Three-level F-type inverter," *IEEE Trans. Power Electron.*, early access, Apr. 6, 2021, doi: 10.1109/TPEL.2021.3071359.
[19] M. Podgórna, M. Ptak, M. Chrunik, I. Jankowska-Sumara, J. Piecha, and D. Zasada, "The investigations of phase transitions in the (1-x)$PbZrO_3$-x$BiFeO_3$ nanocrystals using differential scanning calorimetry and Raman spectroscopy," *J. Appl. Phys.*, vol. 124, no. 5, Aug. 2018, Art. no. 054102.
[20] K. Gładyk, W. Piecek, M. Czerwiński, P. Morawiak, M. Chrunik, and Z. Raszewski, "An effect of chiral dopants on mesomorphic and electro-optical properties of ferroelectric smectic mixture," *Liquid Crystals*, vol. 46, no. 15, pp. 2134–2148, Dec. 2019. [Online]. Available: https://www.tandfonline.com/doi/full/10.1080/02678292.2019.1613689
[21] L. Yan, D. Liu, H. Lan, and Z. Jiao, "Compact traveling wave micromotor based on shear electromechanical coupling," *IEEE/ASME Trans. Mechatronics*, vol. 21, no. 3, pp. 1572–1580, Jun. 2016.
[22] L. Wang, V. Hofmann, F. Bai, J. Jin, and J. Twiefel, "Modeling of coupled longitudinal and bending vibrations in a sandwich type piezoelectric transducer utilizing the transfer matrix method," *Mech. Syst. Signal Process.*, vol. 108, pp. 216–237, Aug. 2018.
[23] S. He, S. Shi, Y. Zhang, and W. Chen, "Design and experimental research on a deep-sea resonant linear ultrasonic motor," *IEEE Access*, vol. 6, pp. 57249–57256, 2018.
[24] K. Spanner and B. Koc, "Piezoelectric motors, an overview," *Actuators*, vol. 5, no. 1, p. 6, Feb. 2016. [Online]. Available: http://www.mdpi.com/2076-0825/5/1/6
[25] X. Tian, Y. Liu, J. Deng, L. Wang, and W. Chen, "A review on piezoelectric ultrasonic motors for the past decade: Classification, operating principle, performance, and future work perspectives," *Sens. Actuators A, Phys.*, vol. 306, May 2020, Art. no. 111971.
[26] X. Yang, Y. Liu, W. Chen, and J. Liu, "Sandwich-type multi-degree-of-freedom ultrasonic motor with hybrid excitation," *IEEE Access*, vol. 4, pp. 905–913, 2016.
[27] D. Bai, Q. Quan, D. Tang, and Z. Deng, "Design and experiments of a novel rotary piezoelectric actuator using longitudinal–torsional convertors," *IEEE Access*, vol. 7, pp. 22186–22195, 2019.
[28] J. Wu, Y. Mizuno, and K. Nakamura, "Piezoelectric motor utilizing an alumina/PZT transducer," *IEEE Trans. Ind. Electron.*, vol. 67, no. 8, pp. 6762–6772, Aug. 2020.
[29] R. Ryndzionek, M. Michna, M. Ronkowski, and J.-F. Rouchon, "Chosen analysis results of the prototype multicell piezoelectric motor," *IEEE/ASME Trans. Mechatronics*, vol. 23, no. 5, pp. 2178–2185, Oct. 2018.
[30] R. Ryndzionek, M. Ronkowski, M. Michna, L. Sienkiewicz, and J.-F. Rouchon, "Design, modelling and analysis of a new type of piezoelectric motor. Multicell piezoelectric motor," in *Proc. IECON 39th Annu. Conf. IEEE Ind. Electron. Soc.*, Nov. 2013, pp. 3910–3915.
[31] R. Ryndzionek, M. Michna, M. Ronkowski, and J.-F. Rouchon, "Analytical modelling of the multiceli piezoelectric motor based on three resonance actuators," in *Proc. IECON 40th Annu. Conf. IEEE Ind. Electron. Soc.*, Oct. 2014, pp. 2701–2705.
[32] R. Ryndzionek, Ł. Sienkiewicz, M. Michna, and F. Kutt, "Design and experiments of a piezoelectric motor using three rotating mode actuators," *Sensors*, vol. 19, no. 23, p. 5184, Nov. 2019. [Online]. Available: https://www.mdpi.com/1424-8220/19/23/5184
[33] D. Stoia, E. Linul, and L. Marsavina, "Influence of manufacturing parameters on mechanical properties of porous materials by selective laser sintering," *Materials*, vol. 12, no. 6, p. 871, Mar. 2019. [Online]. Available: https://www.mdpi.com/1996-1944/12/6/871

ROLAND RYNDZIONEK (Member, IEEE) received the M.Sc. degree in electrical engineering from the Gdańsk University of Technology (GUT), Gdańsk, Poland, in 2010, the M.Sc. degree in electrical engineering from INP-ENSEEIHT, Toulouse, France, in 2012, and the joint Ph.D. degree in electrical engineering from GUT and INP, in 2015. From 2015 to 2017, he was a Postdoctoral Research Engineer with SuperGrid Institute, Lyon, France. Since 2017, he has been with GUT, where he is currently an Assistant Professor. His scientific and research interests include development of piezoelectric motors for embedded applications, designing of the mechatronic structures, and power converters.

ŁUKASZ SIENKIEWICZ received M.Sc. degree in electrical engineering from the Gdańsk University of Technology (GUT), in 2010, the M.Sc. degree from INP-ENSEEIHT (INPT), Toulouse, France, in 2012, with a focus on advanced mechatronics, and the dual Ph.D. degree in electrical engineering from GUT and INPT, in 2016. Since 2014, he has been working with the Faculty of Electrical and Control Engineering, GUT. His main scientific and research interests include the design of mechatronic systems, in particular utilizing piezoelectric sensors and actuators, using modern IT techniques (inventor, ansys, matlab/simulink RT, SCADA, and C/C ++/python).

MICHAŁ MICHNA (Senior Member, IEEE) received the M.Sc. and Ph.D. degrees in electrical engineering from the Gdańsk University of Technology (GUT), Poland, in 1999 and 2005, respectively. Since 1999, he has been with GUT, where he is currently an Assistant Professor. His main scientific and research interests include a wide spectrum of mathematical modeling and diagnosis of electrical machines using analytical modeling and FEM-based computations.

MAREK CHODNICKI graduated from the Faculty of Mechanical Engineering, Gdańsk University of Technology (GUT), in 2003. He received the Ph.D. degree from the Faculty of Mechanical Engineering, GUT, in 2011 and the master's degree in Research and Development Project Manager-for Researchers, in 2015. He studied at the TH Köln, Germany, in 2003. His scientific output counts over 39 items, including 22 publications and over 17 unpublished works. He has professional experience in the field of academic competences (apart from the GUT, also the University of Informatics and Management, Olsztyn, Poland, and École Nationale d'Ingénieurs de Metz, France) and engineering (ZELIN Trade Office, Koyo Bearings, U.K., Chomar Engineering-own business, vMACH Engineering GmbH, Germany, and Fullfreshair Ltd.). He organized, supervised, and participated in the implementation of several dozen domestic and foreign projects. He received the PRINCE2 Foundation Project Management Certificate.